

Mechanism for pressure drop variation caused by filtration of diesel particulates

by

Kazuhiro Yamamoto, Yuta Tajima

Dep. Mech. System Eng., Nagoya University

Chikusa, Furo, Nagoya, Aichi-ken 4648603, JP

Correspondence: Kazuhiro YAMAMOTO
Dep. Mech. System Eng.
Nagoya University
Chikusa, Furo, Nagoya, Aichi-ken 4648603, JP
Tel: +81-052-7894471, Fax: +81-052-7894471
E-mail: kazuhiro@mech.nagoya-u.ac.jp

Keywords: Filtration; DPF; Diesel soot; Flow dynamics; Pressure drop

Mechanism for pressure drop variation caused by filtration of diesel particulates

by

Kazuhiro Yamamoto, Yuta Tajima

Dep. Mech. System Eng., Nagoya University

Chikusa, Furo, Nagoya, Aichi-ken 4648603, JP

(Abstract)

Diesel engines have better fuel consumption efficiency than that of gasoline engines. To reduce the particle emission in the diesel exhaust, a ceramic filter, called DPF (diesel particulate filter), has been developed. Unfortunately, the pressure drop (filter backpressure) continues to increase, resulting in an increase in fuel conversion rate as well as available torque. In order to develop the filter with lower pressure drop, the filter structure is strategically optimized in the design of the filter product. To do so, the information on phenomena during the filtration is needed. This paper sets out numerically to study the variation of the pressure drop when the particulates are trapped inside the porous walls of DPF. To discuss the flow dynamics and pressure drop caused by the soot deposition, the numerical simulation is purposely conducted in two dimensional coordinate. This is because the variation of flow channel through pores during the filtration can be visualized easily. Here, eight filters were tested systematically. Utilizing these simulation results, we try to explain the main factors for the pressure drop variation during the filtration. Based on the presented results, it is shown that the flow field is gradually varied during the filtration. The knowledge regarding the well-known pressure drop variation observed in the stage from the depth filtration to the surface filtration is provided.

Introduction

In our daily life, a main energy resource is produced from combustion of oil, coal, and natural gas, which inevitably releases CO₂ to the atmosphere. In general, the transport sector is a significant contributor to CO₂ emission in the world.^{1,2} Due to the global warming, CO₂ emissions should be reduced. It is reported that diesel engines have better fuel conversion efficiency than that of gasoline engines. However, compared with gasoline vehicles, there are more particulate emissions. It is emphasized that emission of diesel soot could potentially penetrate into the lung with human carcinogenic effects.^{4,5} Then, in many countries including Japan, stricter exhaust emission standards such as Euro VI in 2014 have been set.

To reduce the particle emission in the diesel exhaust, a ceramic filter, called DPF (diesel particulate filter), has been developed.⁶ So far, the structure of a monolithic wall-flow type is widely used. Since the filter has porous ceramic walls of SiC or cordierite substrate, the diesel particulates are most simply caught when the exhaust gas including particulates is forced to go through the porous ceramic walls between pores. The filtration efficiency is almost 99 %⁷⁻⁹, although a clean filter generally has much lower filtration efficiency for nuclei mode particles. At the same time, the pressure drop (filter backpressure) continues to increase because of the particle trap inside the filter walls, resulting in the reduction of fuel conversion rate and available

torque.^{2,3,6} Then, we need to decrease the filter backpressure even in driving condition.

In order to develop the filter with lower pressure drop, the filter structure is strategically optimized in the design of the filter product. To do so, the information on phenomena during the filtration is needed.

Typically, the inlet width of the honeycomb filter is roughly 2 mm, and the average size of pores inside the ceramic wall is about 10 μm , at which diesel particulates are trapped. In experiments, it could be practically

impossible to see the particle motion inside filter wall directly. Thus, a numerical simulation is suitable to discuss the filtration. So far, we have intended to conduct numerical simulations of the DPF filtration.¹⁰⁻¹⁶

These simulations have been conducted by a lattice Boltzmann method (LBM), which is suitable for porous media flow. Muntean et al. have simulated the flow in a cordierite filter¹⁷, but have not considered the particle

laden flow for discussing the filtration.

This paper sets out numerically to study the variation of the pressure drop when the particulates are trapped inside the porous walls of DPF. The paper also proposes the mechanism of well-known pressure drop

during the shift from the depth filtration and the surface filtration. To discuss the flow dynamics and pressure drop caused by the soot deposition, the numerical simulation is purposely conducted in two dimensional

coordinate. This is because the variation of flow channel through pores during the filtration can be visualized

easily. Here, several filters were tested systematically. One filter with real pores was obtained by an X-ray CT scanning, corresponding to a reference. **To obtain 2D filter structure where the exhaust gas would pass through, the thin slice of the filter wall was used.** Other seven filters with different pore structure were computational formed. That is, these filter structures were produced by changing the filter structure of the reference filter. Concretely, the porosity as well as the pore size were systematically modified in terms of CT data composing of 0 (pore) and 1 (substrate). This procedure could not be done in the case of the real products. Totally, eight simulations were performed at the same initial conditions and boundary conditions. Utilizing these simulation results, we try to explain the main factors for the pressure drop variation during the filtration. Simultaneously, we can obtain the information for optimizing the filter structure with lower filter backpressure.

Numerical method

Figure 1 shows the two-dimensional calculation domain used for the simulation. The material of the filter was Al_2TiO_5 , and its structure had so-called wall flow monoliths. Although the 3D inner structure of the filter wall obtained by the X-ray CT scanning¹⁰⁻¹⁶, only one slice image of the filter was used for easy data

analysis. The advantage was that it could be much easier to visualize one complex flow pattern normally by identifying soot region simultaneously, because we only needed to focus on one slice image even in the case of the time-dependent phenomena. As for the coordinate in the simulation, the flow direction of the inflow gas passing across the filter wall is set for the X-axis, and another direction normal to the X-axis is defined as the Y-axis. The size of the calculation domain was 0.950 mm (X) \times 0.990 mm (Y). In the simulation, the grid size was 0.0025 mm (2.5 μ m), which was the same value as the spatial resolution of the CT scanning, and the number of grid points was 380 (X) \times 396 (Y). The filter size of 0.670 mm (X) \times 0.990 mm (Y) was placed at the center of the calculation domain, and the width of inlet and outlet zones were 0.210 mm (85 grids) and 0.060 mm (25 grids), which were set upstream and downstream of the filter, respectively.

Figure 2 corresponds to the combined image of the substrate structure of eight filters used in the simulation. The filter properties are shown in Table 1. As already mentioned, Filter 0 of the real filter structure was considered as the reference. Filter 1, in which the total substrate area was shrunk with higher porosity, was termed the front & rear thin filter. Filter 2, in which the total substrate area was expanded with lower porosity, was termed the front & rear thick filter. Filters 3 and 4 were the front thin or front thick filter, with higher or lower porosity than that of Filter 0 in the front section. Filters 5 and 6 were the rear thin or rear thick

filter, with higher or lower porosity in the rear section. These filters were numerically made by shifting the position of the filter surface by one spatial grid. Filter 7 had unique substrate structure whose surface was flattened by cutting the filter wall surface, which was termed the surface flat filter.

Next, the boundary conditions of the flow and concentration fields are explained. Exhaust gas at a temperature of 300°C was evenly flowed from the upstream of the filter wall. The inlet velocity was 3 cm/s.¹² The pressure at the outlet was the constant value of atmospheric pressure. Each boundary for the upper or lower side of the calculation domain were treated as symmetrical boundaries with slip boundaries. A non-slip wall (boundary) was set on the substrate surface of the filter wall. On the other hand, the permeability of the soot layer generally depends on the flow velocity passes through the filter wall, the soot primary particle size, and the diffusion coefficient of aggregate particles.¹⁴

As for the soot concentration field, the mass fraction (concentration) was 0.1 at the inlet. At the upper and lower sides of the calculation domain, the concentration gradient along the Y-axis was zero. At the outlet, a developed boundary condition was adopted, where the gradient of soot concentration along X-axis was zero. Due to the filtration, the soot was trapped on the filter substrate or the soot deposition region. The soot deposition model proposed by Uenishi et al.¹⁸ was adopted. In their model, the soot aggregate particle is

trapped by the Brownian diffusion and the interception effect. In this simulation, the mass of deposited soot was calculated based on the filtration efficiency predicted by their model. Model parameters such as soot diffusion coefficient were the same as the proposed value in the reference.^{19,20} Here, the size of soot aggregate particle was the constant of 100 nm. In order to predict the pressure drop more precisely, the density, the porosity, and the permeability of deposited soot layer were given by considering the size of soot aggregate particle of 100 nm.

Results and discussion

Flow field before soot deposition

Initially, the flow field already appearing before soot deposition was examined. The inflow without soot deposition was considered. We continued the simulation until we achieved the steady state flow. Figure 3 shows the flow field in Filter 0. The red streamline and the filter substrate by gray are described. Additionally, the region of large filtration velocity is shown by the green (> 30 cm/s) and the yellow (> 10 cm/s). The filtration velocity of V is expressed by

$$V=(V_x^2+V_y^2)^{1/2} \quad (1)$$

where V_x and V_y are the velocities in X and Y directions. It is much enlarged at the region of narrow pores between substrates. There are many flow streams automatically forming, showing the tangled flow paths.

Figure 4 illustrates the interrelationship between the porosity and the initial pressure drop, which corresponds to the property of the clean filter before filtration.^{8,9} All values were obtained by the flow simulation without adding soot at the inlet. These values together with the difference between Filter 0 and others are shown in Table 1. The initial pressure drop seems to be smaller when we set the larger porosity of the filter. More specifically, the difference between Filters 1 and 0 is -0.029 kPa and that between Filters 2 and 0 is +0.284 kPa. Therefore, the change in the initial pressure drop is much larger when the porosity decreases than when the porosity increases. This tendency is also confirmed between Filters 3 and 4 or between Filters 5 and 6. It is noted that the initial pressure drop may be dependent on the flow direction. Then, we simulated the flow when the filter was set in the opposite direction to consider the reverse flow. As a result, the value of the initial pressure drop did not change when the flow was reversed. Therefore, the change in the initial pressure drop is larger when the porosity decreases, which could be due to the fact that, for all filters, the averaged porosity is

smaller than 0.5.

Finally, Filter 7 was compared with Filter 0. As shown in Table 1, the difference in the initial pressure drop between Filters 7 and 0 is only -0.001 kPa, and the initial pressure drop of Filter 7 is almost the same as that of Filter 0. Therefore, even though the filter surface is flattened, the initial pressure drop does not change.

Visualization of soot region and pressure drop

Next, the soot deposition process including the transition of the soot deposition region was revealed. First, results of Filters 0, 1, and 2 were compared. Figure 5 displays the soot deposition region at the time of $t = 75$ s. Here, the time of t was counted after we started the simulation. The soot is known to be initially transported deeply into the filter wall, after which pores on the filter surface are plugged with soot. This phenomenon corresponds to the shift from the depth filtration to the surface filtration.^{8,13} Interestingly, it is seen that the soot deposition region is formed in a deeper part of the filter as the entire porosity decreases. It is found that more soot is transported downstream in the earlier stage of the filtration. More importantly, due to the soot deposition, the spacing between substrates is narrower.

It should be noted that, in case of Filter 0, the surface filtration just occurs at $t = 76$ s. For Filters 0, 1, 2,

the maximum filtration velocities shown by Eq. 1 around the filter surface are 21.3, 19.4, 27.6 cm/s, respectively. Since the porosities of these filters are 0.45, 0.50, 0.39, it is found that the filtration velocity increases as the porosity decreases. Therefore, it is concluded that as the porosity decreases, more soot is convected deeply inside the filter due to the enlarged filtration velocity.

Next, we investigated results of filters in which only the porosity of the upper part of the filter wall was altered. By comparing soot deposition region in Fig. 5, a similar distribution is observed between Filters 1 and 3 or between Filters 2 and 4. Additionally, the distribution of soot deposition regions in Filters 5, 6 are similar to that in Filter 0. Then, the impact of the porosity of the downstream filter region on the soot deposition process is found to be very small. On the other hand, by comparing Filters 0, 3, 4, or Filters 1 and 5, or Filters 2 and 6, more soot is transported downstream. Therefore, it is revealed that only the porosity in the front section of the filter affects the soot deposition region. This is because more soot is efficiently trapped around the filter wall surface even in the case of the depth filtration^{8,13} (see Fig. 5).

Moreover, the effect of flattening the filter surface was examined. As shown in Figs. 5(a) and 5(h), the soot region inside the Filter 7 is quite similar to that of Filter 0. The only difference is that the shape of the soot layer in upstream of Filter 7 differs from that of Filter 0, because the filter surface is totally flat. By considering

the fact that the pressure drop before the filtration in Filter 7 almost matches that of Filter 0, effects of surface flatterer is minimal for reducing the pressure drop or improving the filtration efficiency. Hence, further investigation on Filter 7 was not conducted.

Next, the temporal change in the pressure drop during the filtration was examined. Figure 6 shows the typical temporal change in the pressure drop. The profiles of Filters 0 and 5 or Filters 1 and 3 are almost matched. First, results of Filters 0, 1, and 2 were compared. In general, when the soot attaches inside the pores of the filter, the flow area becomes narrower. Before long, a bridge is formed at the inlet of the flow path, resulting in filter plugging. As illustrated in Fig. 6, the pressure increasing rate is forced to be changed, which is the well-known variation in pressure drop profile during the soot deposition.^{8,9,11} The first rapid increase is caused by the depth filtration. When the formation of bridging on all flow paths is completed, the soot deposition region is moved from the downstream to the upstream of the filter wall. Since these phenomena are observed for all filters, the time-dependent of the pressure drop is quite similar. It should be noted that, for each filter, the degree of the pressure rise due to the soot deposition is found to be different, simply because each filter has different porosity.

As discussed on Fig. 5, the pressure drop during the filtration must be affected by the local porosity of

the front section. First, based on the temporal change in the pressure drop, the impact of porosity in the front section was revealed. By comparing profiles of Filters 0, 3, 4, it is found that, when the porosity of the upstream of the filter wall is smaller, the time toward the shift to the surface filtration is shorter. Therefore, an increase in the pressure drop occurs earlier by the reduction of the porosity in the front section. On the other hand, by comparing profiles of Filters 0, 5, 6, the effect of porosity in the rear section could be evaluated. It is seen that the profiles of Filters 0 and 5 are almost the same. The pressure difference between Filters 0 (or 5) and 6 correspond to the difference between initial pressure drops. Therefore, as far as the pressure increase during the filtration is concerned, the impact the rear porosity of the filter wall could be negligible.

Change in the flow field due to soot deposition

Finally, focusing on the flow field, we discussed the pressure variation during the filtration. Expectedly, when the soot deposition proceeds, resultant spacing between substrates is always decreasing inside the filter. Thus, the relationship between the maximum filtration velocity and the pressure drop was examined. Results are shown in Fig. 7, obtained for Filter 0. As more soot is deposited, pores used for the flow path is narrower. Then, the filtration velocity would be monotonically larger and larger, with higher pressure drop. However, as

seen in this figure, the maximum filtration velocity takes its peak at $t = 76$ s. It is the moment when the passage from the depth filtration to the surface filtration occurs. Based on the result in Fig. 7, it seems that, once the surface filtration starts, the maximum velocity gradually goes back to the initial value before the soot deposition. Then, the pressure drop during the filtration is closely related with the temporal change of the flow field.

For detailed discussion, we examined the time-variation of the flow streams appearing in the filter. Figure 8 illustrates the flow field of Filter 0 obtained at $t = 0, 60, 167$ s. To visualize the flow path inside the filter, the maximum filtration velocity is set to be 10 cm/s. Figure 9 shows the definition of each channel in Filter 0, named by the flow path number on the filter surface. As seen in Fig. 8, there are eight channels at the filter surface. We monitored the flow rate through each channel. Since the simulation in this study is two-dimensional, the flow rate through the channel is the value per unit length ($\text{m}^3/\text{m}\cdot\text{s}$). Results are shown in Fig. 10.

Again, we should emphasize that the flow rate along each channel is temporally changing. Initially, as confirmed in Fig. 8(a), the main channel with the high flow rate is channel 7. This could be because its inlet width is relatively large so that it is affordable with multiple flow paths in downstream. Additionally, the flow path through channel 7 is relatively straight. Expectedly, the pressure drop through this channel is small.

However, the soot is favorably deposited along this channel, and gradually, it is more difficult for the flow to go through, which causing the larger pressure drop along this channel. If there is another channel where the flow can pass through easily, the local flow field is automatically changed. In other words, the flow selects the channel with less pressure drop. That is why the flow rate along the channel 7 becomes inevitably reduced, whereas the flow rates of other channels are conversely enlarged. As seen in this figure, after $t = 40$ s, even the flow rates of channels 3 and 6 turn to decrease, which could be also due to the soot deposition along these channels. By comparing Figs. 8(a) and 8(b), the filtration velocity at $t = 60$ s through channels 3, 6, 7 is much lower than the original value. Later, the flow rates of all channels except for channel 1 decrease. That means most of flow concentrates only on the channel 1, because other channels are already plugged with soot.

After the inlet pore of channel 1 is lastly plugged, the flow rate of channel 1 takes a peak at $t = 76$ s, at which the transition from the depth filtration to the surface filtration occurs. At this moment, all flows are forced to pass through the soot deposition region, and almost all the flow rates of other channels turn to increase, again.

Interestingly, as seen in Fig. 8(c), the filtration velocity through each channel is close to each other, because the thick soot layer is formed in front of the filter inlet to have the flat velocity distribution. After that, the pressure drop linearly increases as the soot layer becomes thicker. This tendency is observed for all filters.

Thus, the well-known pressure drop variation observed in the stage from the depth filtration to the surface filtration is explained by the resultant change of the flow across the filter wall. This information is quite useful for the design of filter with low pressure drop by optimizing the inner porous structure.

Conclusions

We numerically investigated the impact of the filter substrate structure on the soot deposition process.

The numerical simulation was conducted in two dimensional coordinate. One filter with real pores obtained by the CT scanning was used as a reference, and other seven filters with different pore structure were computational formed, in order to obtain the information for optimizing the filter structure with lower filter backpressure. Main findings of the present numerical simulation are:

1. The initial pressure drop is apparently smaller when we set the larger porosity of the filter. The change in the initial pressure drop is much larger when the porosity decreases than when the porosity increases.

When the surface of the filter is intentionally flattened, the initial pressure drop does not change.

2. When the soot deposits inside the filter wall, the spacing of substrate pores is narrower, which makes the pressure drop higher. By discussing the location of soot deposition region, the impact of the porosity in

the rear (downstream) part of the filter wall could be negligible, whereas that in the front (upstream) part seems to be highly influential. This is because the soot always deposits around the filter surface even during the depth filtration. Resultantly, by reducing the porosity of the upstream of the filter wall, the time toward the shift to the surface filtration can be shorter.

3. Due to the soot deposition, it is always observed that there are some channels with decreasing flow rate and others with increasing flow rate. The fact that the flow selects the channel with less pressure drop is an important finding in the filtration process. When the surface filtration occurs, the thick soot layer is formed in front of the filter inlet to have the flat velocity distribution, showing the linear dependent of the pressure drop on the soot layer thickness. Thus, the well-known pressure drop variation observed in the stage from the depth filtration to the surface filtration is explained by the resultant change of the flow across the filter wall.

Acknowledgements

A part of this work was supported by AICE, the Research association of Automotive Internal Combustion Engines, in Japan.

References

1. Zervas E, Pouloupoulos S and Philippopoulos C. CO₂ emissions change from the introduction of diesel passenger cars: Case of Greece. *Energy* 2006; 31: 2579-2589.
2. Knecht W. Diesel engine development in view of reduced emission standards. *Energy* 2008; 33: 264-271.
3. Schaefer-Sindlinger A, Lappas I, Vogt CD, Ito T, Kurachi H, Makino M and Takahashi A. Efficient material design for diesel particulate filters. *Topics in Catalysis* 2007; 42-43: 307-317.
4. Johnson JE and Kittelson DB. Deposition, diffusion, and adsorption in the diesel oxidation catalyst. *Applied Catalysis B: Environmental* 1996; 10: 117-137.
5. Kennedy IM. The health effects of combustion-generated aerosols. *Proc. Combust. Inst.* 2007; 31: 2757-2770.
6. Johnson TV. Vehicular emissions in review. *SAE Int. J. Engines* 2016; 9: 1258-1275.
7. Adler, J. Ceramic diesel particulate filters. *International Journal of Applied Ceramic Technology* 2005; 2: 429-439.
8. Wirojsakunchai E, Schroeder E, Kolodziej C, Foster DE, Schmidt N, Root T, Kawai T, Suga T, Nevius T

- and Kusaka T. Detailed diesel exhaust particulate characterization and real-time DPF filtration efficiency measurements during PM filling process. *SAE Technical Paper* 2007-01-0320, 2007.
9. Tsuneyoshi K, Takagi O and Yamamoto K. Effects of washcoat on initial PM filtration efficiency and pressure drop in SiC DPF. *SAE Technical Paper* 2011-01-0817, 2011.
 10. Yamamoto K, Satake S, Yamashita H, Takada N and Misawa M. Lattice Boltzmann simulation on porous structure and soot accumulation. *Math. Comp. Sim.*, 2006; 72: 257-263.
 11. Yamamoto K and Nakamura M. Simulation on flow and heat transfer in diesel particulate filter. *ASME J. Heat Transfer* 2011; 133(6): DOI:10.1115/1.4003448.
 12. Yamamoto K and Yamauchi K. Numerical simulation of continuously regenerating diesel particulate filter. *Proc. Combust. Inst.* 2013; 34: 3083-3090.
 13. Yamamoto K and Ohori S. Simulation on flow and soot deposition in diesel particulate filter. *Int. Engine Research* 2013; 14: 333-340.
 14. Yamamoto K and Sakai T. Simulation of continuously regenerating trap with catalyzed DPF. *Catalysis Today* 2015; 242: 357-362.
 15. Yamamoto K and Toda Y. Numerical study on filtration of soot particulates in gasoline exhaust gas by SiC fiber filter. *Key Engineering Materials* 2017; 735: 119-126.

16. Kong H and Yamamoto K. Simulation on soot deposition in in-wall and on-wall catalyzed diesel particulate filters. *Catalysis Today* 2018, in press.
17. Muntean GG, Rector D, Herling D, Lessor D, Khaleel M. Lattice-Boltzmann diesel particulate filter sub-grid modeling - A progress report. *SAE Technical paper* 2003-01-0835, 2003.
18. Uenishi T, Tanaka T, Shigeno G, Fukuma T, Kusaka J, Daisho Y. A quasi two dimensional model of transport phenomena in diesel particulate filters- the effects of particle and wall pore diameter on the pressure drop. *SAE Technical paper* 2015-01-2010, 2015.
19. Gutfinger C, Tardos GI. Theoretical and experimental investigation on granular bed dust filters. *Atmospheric Environment* 1979; 13(6): 853-867.
20. Konstandopoulos AG and Skaperdas E. Microstructural properties of soot deposits in diesel particulate traps. *SAE Technical paper* 2002-01-1015, 2002.

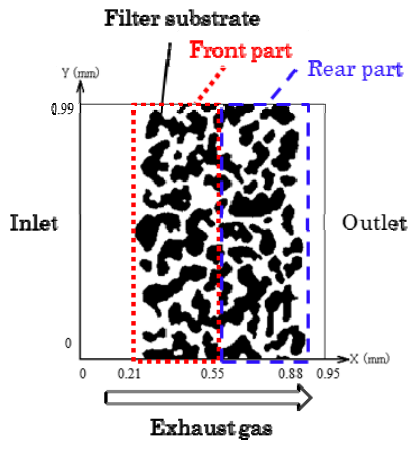


Fig. 1 Calculation domain with coordinate

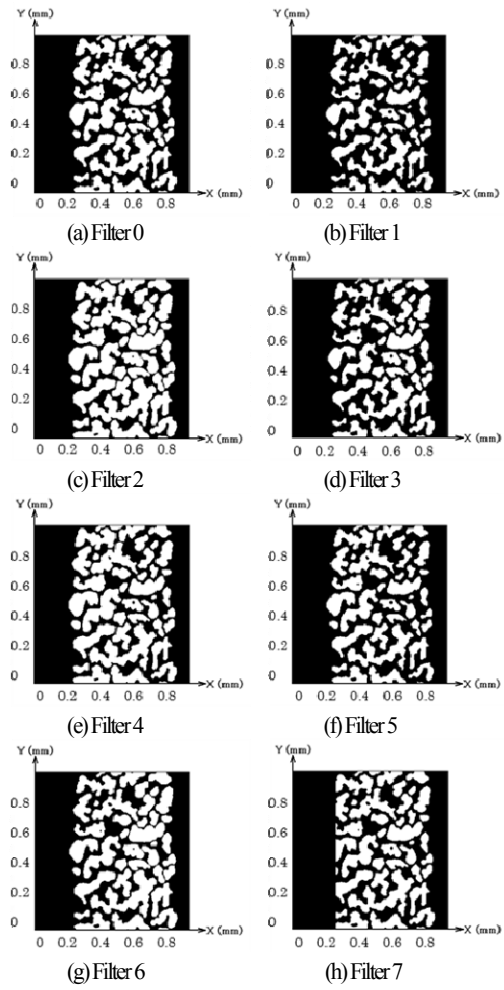


Fig. 2 Substrate structure of filters 0 to 7

Table 1 Porosity and initial pressure drop

Filter No. & name	Porosity $\epsilon_{ALL}(\epsilon_f, \epsilon_r)$	Initial pressure drop (difference)
0 Reference	0.45 (0.45, 0.45)	0.081 kPa (-)
1 Front & rear thin	0.50 (0.50, 0.51)	0.052 kPa (-0.029)
2 Front & rear thick	0.39 (0.40, 0.39)	0.365 kPa (+0.284)
3 Front thin	0.48 (0.50, 0.45)	0.068 kPa (-0.013)
4 Front thick	0.42 (0.40, 0.45)	0.151 kPa (+0.070)
5 Rear thin	0.48 (0.45, 0.51)	0.063 kPa (-0.018)
6 Rear thick	0.42 (0.45, 0.39)	0.241 kPa (+0.160)
7 Surface flat	0.45 (0.45, 0.45)	0.080 kPa (-0.001)

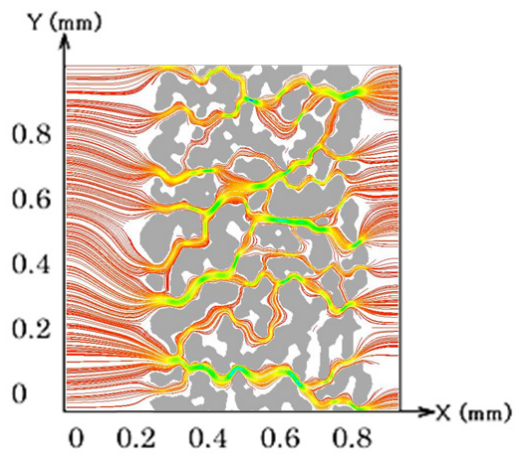


Fig. 3 Flow field shown by streamline in Filter 0

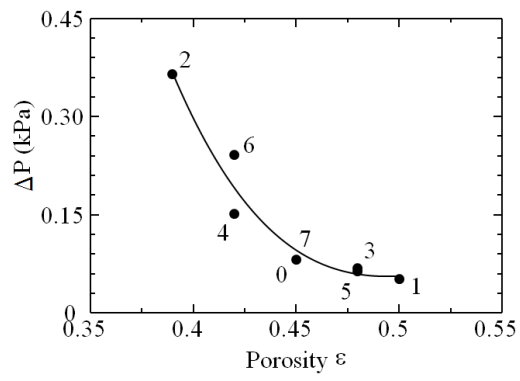


Fig. 4 Relations of porosity and initial pressure drop

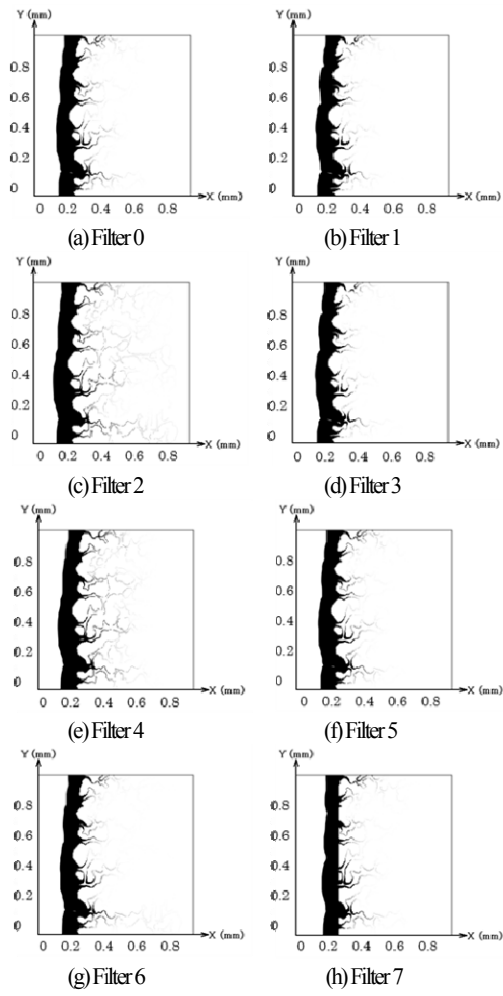


Fig. 5 Soot deposition region at $t = 75$ s for all filters.

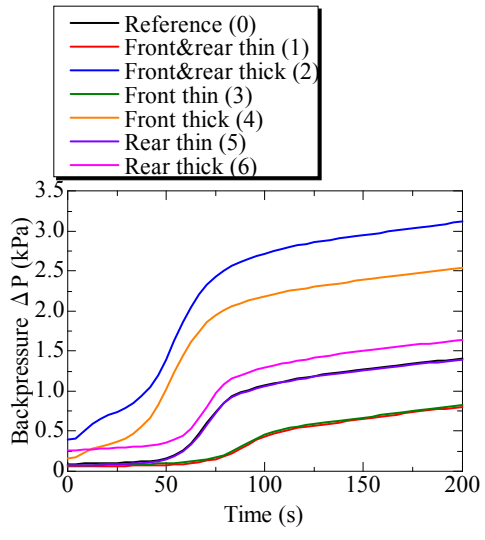


Fig. 6 Time-variation of the pressure drop

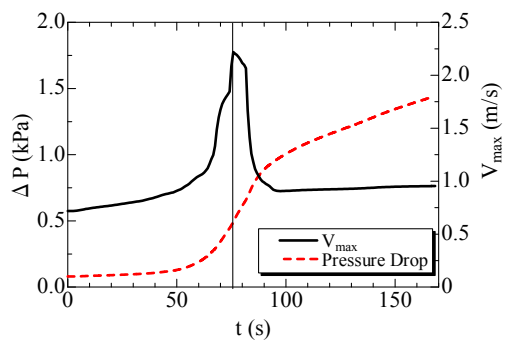


Fig. 7 The maximum filtration velocity and the pressure drop inside Filter 0

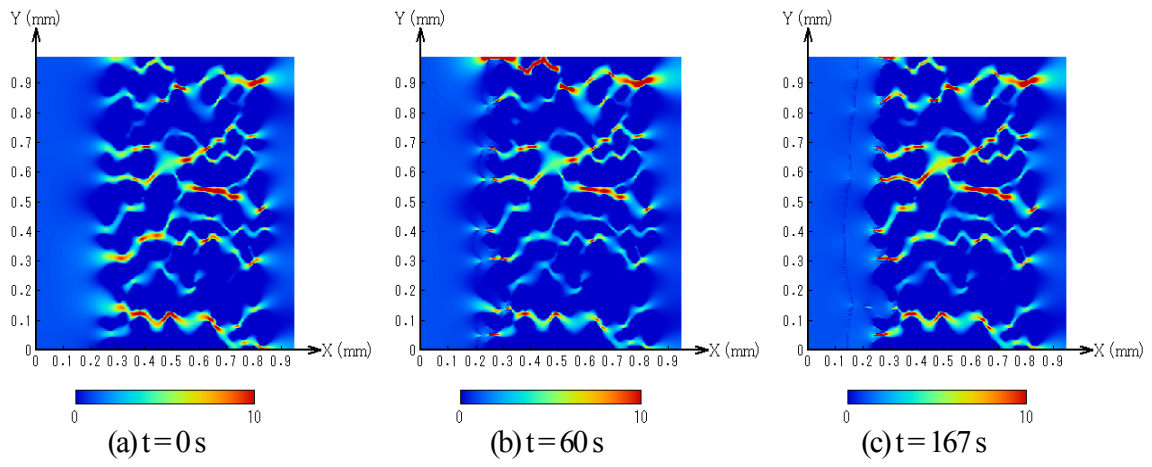


Fig 8 Distribution of filtration velocity inside Filter 0 at different time

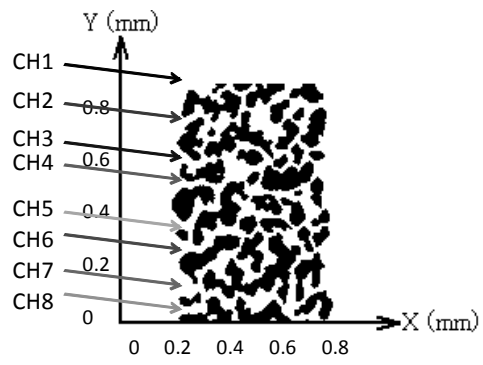


Fig. 9 Definition of each channel in Filter 0, named by the flow path number on the filter surface

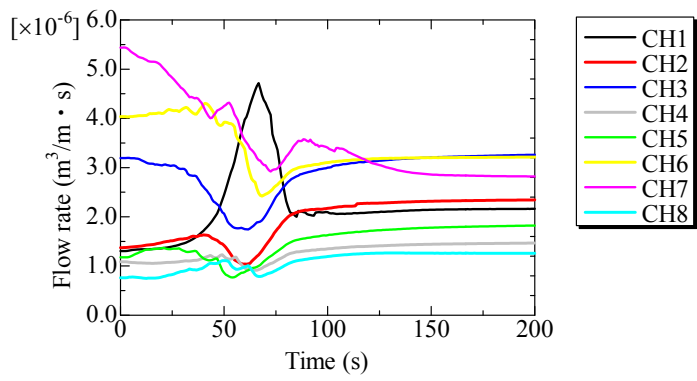


Fig. 10 Evaluation of flow stream by monitoring flow rate through the front pores named by channel number of Filter 0